Cement and Concrete Research 162 (2022) 107009

Contents lists available at ScienceDirect

Cement and Concrete Research

journal homepage: www.elsevier.com/locate/cemconres

Self-cleaning performance of photocatalytic cement mortar: Synergistic effects of hydration and carbonation

Daoru Liu [a,b], Anna Kaja [b], Yuxuan Chen [a,b], H.J.H. Brouwers [b], Qingliang Yu [a,b,*]

[a] School of Civil Engineering, Wuhan University, Wuhan 430072, China
[b] Department of the Built Environment, Eindhoven University of Technology, P. O. Box 513, 5600 MB Eindhoven, the Netherlands

ARTICLE INFO

Keywords:
Self-cleaning property
Band energy
Phase composition
Pozzolanic reaction
TiO_2-SiO_2 composite

ABSTRACT

The prospect of nano-photocatalysts in cementitious systems is promising but the engineering application is still limited, caused by the insufficient insights on durability properties during the service. Mortars with different binders and photocatalysts are prepared and characterized to investigate the deterioration mechanisms of self-cleaning performance upon simultaneous hydration/carbonation. Alterations in self-cleaning performance driven by the change of microstructure, phase composition, and optical properties are analyzed. The drop in self-cleaning performance is attributed to the higher band energy with surface modification, stronger "sheltering" with solid volume increase, worsened mass transfer with reduction of gel pores, and retardation of chemical equilibrium. TiO_2-SiO_2 composite photocatalysts and microsilica were found to resist the deterioration of self-cleaning performance upon hydration/carbonation by promoting mass transfer and chemical equilibrium and limiting surface modification. Finally, a solution to alleviate the deterioration of self-cleaning property, with the consideration on mechanical, erosion properties and cost issues, is proposed.

1. Introduction

Efforts have been devoted to functionalizing building materials in recent decades [1–3]. Functions like air purification and self-cleaning are empowered to cement-based composites by the application of nanosized photocatalysts [4–7]. These two functions are extensively studied in both lab-scale and real-scale, and the deterioration of photocatalytic properties has been observed during the engineering service [8–10]. For lab-scale studies, cementitious specimens modified by photocatalysts are generally sealed and cured for a certain period, before further characterization and analysis [11–13]. However, carbonation could already occur in engineering applications right after the demoulding. The early-age carbonation inevitably affects the hydration process, especially by the so-called "sheltering" effect of carbonation products [9,14,15]. This gap could cause improper interpretation of laboratory results to practice [14]. Hence, the synergistic effect of hydration and carbonation, especially in the early stage (e.g. 7d and 14d), should be well understood to promote practical applications.

The degradation in photocatalytic property upon hydration and carbonation is generally attributed to two effects: 1) the "occupation" effect of active sites by hydration/carbonation products at the early stage, and 2) the "sheltering" effect of the dense layer on the photocatalyst surface due to the accumulation of hydration/carbonation products [9,11,12,16]. However, these two effects can not explain the durable photocatalytic property when rich reactive silica exists [11,17]. Kinetically, the photocatalytic performance is controlled by the semiconductor properties of photocatalysts (band energy, light absorption) and TiO_2-surrounded media (pH, microstructure, ion conditions, etc.) [9,12,18–21]. With hydration/carbonation, these properties would be significantly altered [9,11]. Self-cleaning performance, as the key property of photocatalytic cementitious materials, has been extensively investigated in photocatalysts synthesis and photocatalytic kinetics [22–28]. However, the deterioration of self-cleaning performance upon hydration/carbonation has been rarely investigated in depth [29].

Meanwhile, widely applied photocatalyst, anatase TiO_2, has shown two drawbacks: reduction of surface area due to the agglomeration during wet mixing and high cost [12]. Low-cost composite photocatalysts (e.g. TiO_2-SiO_2) can be synthesized with desirable photocatalytic properties, by partially replacing TiO_2 with other fine particles like nanosilica with exceptional surface properties [30,31]. The synthesis of TiO_2-SiO_2 composites has attracted attention, and various related works have been conducted, especially composite photocatalysts

* Corresponding author at: School of Civil Engineering, Wuhan University, Wuhan 430072, China.
E-mail address: q.yu@bwk.tue.nl (Q. Yu).

https://doi.org/10.1016/j.cemconres.2022.107009
Received 29 January 2022; Received in revised form 5 October 2022; Accepted 9 October 2022

with the "TiO_2@SiO_2 Core-Shell" structure owing to the high photocatalytic activity [30,32–35]. However, current studies on the addition of TiO_2-SiO_2 composites to cementitious systems are mainly on the hydration kinetics, mechanical properties, and early-stage photocatalytic activity, rarely on durability issues [30,31,35]. The existence of reactive silica in TiO_2-SiO_2 composites could affect the evolution of self-cleaning performance upon hydration/carbonation. Nevertheless, this has not been investigated. Meanwhile, the physical agglomeration of fine particles in cementitious systems can be restrained by the addition of surfactant Triton X-405, without change in hydration products [36,37].

Physicochemical changes of cementitious matrix upon hydration/carbonation would considerably affect the photocatalytic performance. However, the relationships between self-cleaning property and hydration/carbonation have not been systematically studied. Moreover, the deterioration mechanisms, considering both photocatalysts and the surrounding media caused by hydration/carbonation, are still missing. Therefore, the synergistic effects of hydration and carbonation of cement composites containing photocatalysts are studied in this study to fill the gaps. Two series of mortars incorporating three photocatalysts are prepared, processed, and characterized. Microstructure, phase composition, optical property, and self-cleaning property of photocatalytic mortars under hydration and carbonation are analyzed and discussed. The results are expected to reveal the deterioration mechanisms of self-cleaning performance upon hydration and carbonation and support the application of photocatalytic cementitious materials.

2. Materials & methods

2.1. Materials

2.1.1. Photocatalysts

One commercial photocatalyst Aeroxide P25 (Evonik Industries), and two self-synthesized photocatalysts (nanoSiO_2-TiO_2 composite, ST, and SiO_2 aerogel-TiO_2 composite, AT) with the (pseudo) "TiO_2@SiO_2 Core-Shell" structure are investigated. The synthesis method has been reported in our previous studies [13,38]. In this study, titanium (IV) isopropoxide 97 % (Sigma-Aldrich) is used as the Ti-precursor, while nanoSiO_2 (EuroSupport) and SiO_2 aerogel (LC 3110, Cabot) are used as the support. The performance of the synthesized photocatalyst using the same recipe was also validated by our previous studies [11,13]. The setup for photocatalysts synthesis and the synthesized composites are shown in Fig. 1. It should be noted here that the ratio of TiO_2 dosage of P25:synthesized composites is 5:1.

2.1.2. Mix design of mortars

CEM I 42.5 N Portland cement (ENCI), microsilica (920ED, Elkem), and standard sand (Normensand) are used for mortar preparation. In total, 2 series and 6 mixes are prepared, as shown in Table 1. Microsilica as the binder is used to promote the pozzolanic reaction and transform the CH to C-S-H. The minimum mass ratio of microsilica/cement is about 26.3 wt%, under the assumption that cement only contains C_3S. This simplification is validated by Naber's experiments [39–41]. There was just a little CH remaining after 28d hydration when 25 wt% of OPC was substituted by microsilica [11,41,42]. Photocatalysts are incorporated with the dosage at 5 wt% of binders. The polycarboxylate-based superplasticizer (SP) (ViscoFlow-37, Sika) is used to adjust the consistency of the fresh mixtures. The non-ionic surfactant (Triton X-405, Dow Chemical) at 0.5 wt% of binders is used for sufficient dispersion of photocatalysts [36,43]. It should be noted here that the cement used in this study has little sodium and no potassium to minimize the impact of Na^+ and K^+ on the pH variation of the pore solution.

2.2. Mortar preparation

2.25 g of the surfactant is first mixed with 100 g of deionized water to prepare the aqueous solution. Photocatalysts are mixed with the solution by an ultrasonic device for 30 min (20 ± 3 °C). SP is mixed with the residual water prior to sample preparation. The mixing of the mortars is performed following the EN 196–1:2005 standard. After mixing, mortars are cast into 4 × 4 × 16 cm^3 molds, then covered by plastic foils for 1d to prevent moisture loss and CO_2 exposure. After that, all samples are demolded, plastic foil enclosed, and stored in a humidity chamber (>90 % RH, 20 °C) for curing (7d, 14d, and 28d). Samples with different hydration ages combined with carbonation are set to investigate the synergistic impact of hydration and carbonation. After curing, samples of each mix design are cut into 10 slices (4 × 4 × 1 cm^3). 5 slices are immersed in isopropanol (200 mL each) to cease the hydration for further characterization. The isopropanol is replaced after 1d and for another 7d. Another 5 slices are sealed with self-adhesive aluminum foils except for the 4 × 4 cm^2 surface and moved to the climate chamber for accelerated carbonation.

2.3. Methodology

2.3.1. Light scattering analysis

The dispersion capacity of surfactant Triton X-405 of fine particles is tested by the light scattering analysis (LSA). Before LSA tests, each sample of 2 g fine particles is dispersed in two aqueous solutions (with/without the surfactant). Then, the agglomeration and dispersion of fine

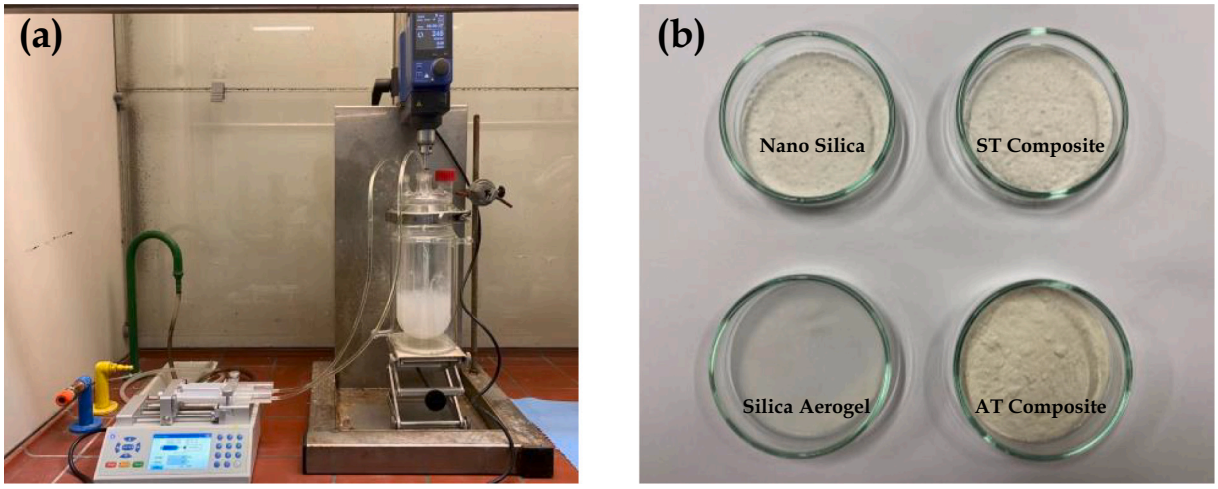

Fig. 1. (a) Setup for photocatalysts synthesis, (b) powders of raw materials and composites (silica aerogel powders of uniform thickness is transparent).

Table 1
Mix design of mortars.

Group	Sample	Binder [g]		Photocatalysts [g]			Additive [%]		Sand [g]	w/b ratio
		Cement	Microsilica	P25	NT	AT	SP	X-405		
Control	Cp	450	/	22.5	/	/	0.4	0.5	1350	0.5
	Cn	450	/	/	22.5	/	0.4	0.5	1350	0.5
	Ca	450	/	/	/	22.5	0.4	0.5	1350	0.5
Hybrid	Sp	337.5	112.5	22.5	/	/	0.9	0.5	1350	0.5
	Sn	337.5	112.5	/	22.5	/	0.9	0.5	1350	0.5
	Sa	337.5	112.5	/	/	22.5	0.9	0.5	1350	0.5

Note: C refers to cement; S refers to microsilica; p refers to P25 photocatalyst; n refers to TiO_2-SiO_2 composite; a refers to SiO_2 aerogel-TiO_2. For example, Cp is the sample prepared by 450 g OPC and 22.5 g P25 photocatalyst; Sa is the sample prepared by 337.5 g OPC, 112.5 g microsilica, and 22.5 g SiO_2 aerogel-TiO_2 photocatalyst.

particles in solutions are observed by the Mastersizer 2000 (Malvern).

2.3.2. Accelerated carbonation

Sealed slices are placed in the carbonation chamber for 28d, with artificial conditions of 3 % CO_2 concentration, 65 % relative humidity (RH), and 20 °C to conduct the one-dimensional accelerated carbonation [11]. After carbonation, an aqueous phenolphthalein solution (1 wt%) is used to observe the carbonation depth.

2.3.3. Fourier-transform infrared spectroscopy (FT-IR), X-ray diffraction (XRD), & thermogravimetric analysis (TGA)

The phase composition of photocatalyst-blended mortars (PCBMs) is analyzed by a XRD machine (D4, Bruker) and TGA (STA 449 F1 Jupiter, Netzsch). The XRD machine runs with a Co tube (40 kV, 40 mA), scanning interval of 0.02°/min, residence time of 0.5 s, and 2θ from 10° to 90°. About 50 mg of ground powders of each sample are heated from 40 to 1000 °C at the rate of 5 °C/min using N_2 as the protective gas. An FT-IR spectrometer (Frontier, PerkinElmer) is applied to analyze the chemical bonds of the synthesized photocatalysts, from 1400 cm^{-1} to 4000 cm^{-1} with a resolution of 1 cm^{-1}.

2.3.4. Nitrogen adsorption/desorption (NAD) & mercury intrusion porosimetry (MIP)

The specific surface area of raw materials and synthesized photocatalyst is analyzed by NAD (TriStar II 3020, Micromeritics) at −196 °C. Samples are dried and degassed at 40 °C under N_2 flow for 4 h, prior to NAD tests. For MIP measurements, crushed pieces with the diameter of 3–4 mm are collected before and after carbonation, respectively. A mercury porosimeter (AutoPore V, Micromeritics), working with the absolute pressure from 0.7 kPa to 420 MPa (0.10 to 61,000 psia) and a contact angle of 130° is used to identify the porosity and pore size distribution.

2.3.5. Scanning electron microscope (SEM)

SEM is used to observe the microstructure and micromorphology. Extracted specimens are gold-coated by a sputter coater (K550X, Emitech) at a current of 65 mA (60 s). Micrographs are recorded by an SEM EMU 220A (Jeol/Holon) with an accelerating voltage of 15 kV.

2.3.6. Optical & self-cleaning properties

The self-cleaning property is related to the optical property of the mortar surface [44,45]. The diffused reflection spectra of mortar plates are measured by a UV-VIS-NIR (Lambda 750, Perkin Elmer) with a 150 mm integrating sphere, at the range of 250–800 nm, with the scan speed of 2 nm/s [12,46–48]. The self-cleaning performance is characterized by the discoloration test with a UV-VIS spectrometer (USB4000, Ocean optics).

The top surface of mortars is polished with a series of SiC sandpapers (P250, P400, P600, P1200, and P2500) before the characterization of the self-cleaning property. The polished surface was firstly washed with deionized water and then cleaned by a high-pressure blower to remove the debris. Each processed surface is stained by spraying the Rhodamine b (RhB) solution (0.1 mM) and then put in a dark environment for overnight natural drying at about 20 °C. For one RhB-stained surface, 9 evenly distributed points are tested 4 times and the average color value is used. Samples are exposed to a UV lamp at the density of 10 ± 0.05 W/m^2 (0, 15, 45, 105, 225, 345, 1365, 1785, and 2800 min), and then the discoloration of the sample is directly obtained by measuring the test points with the spectrometer. In this study, the wavelength range of 380–780 nm and the CIE Lab color a^* for RhB are adopted [11]. The discoloration of a^* is calculated by:

$$\varphi = (a^*_0 - a^*_t)/a^*_0 \times 100\% \quad (1)$$

where φ is the color change of the mortar surface [%], a^* 0 is the value of a^* before UV irradiation, a^* $t$is the value of a^* at t with UV irradiation.

3. Results

3.1. Chemical bonds of synthesized photocatalysts

Fig. 2 shows the FT-IR spectra of the synthesized photocatalysts. Absorption peaks at 947 cm^{-1} and 965 cm^{-1} are observed, while the absorption peak in the range from 900 cm^{-1} to 975 cm^{-1} can be recognized as the Ti-O-Si bonds [49]. The shift of the FT-IR peaks might be attributed to the variation of Ti-O-Si bond angles, due to the different hybridization of bridging oxygen [50].

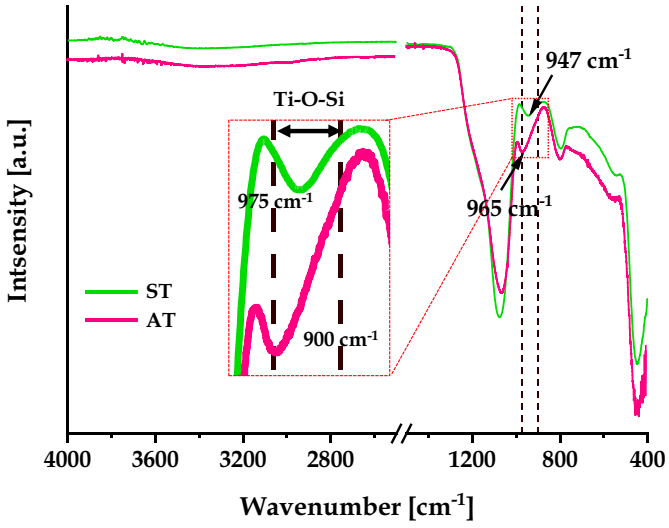

Fig. 2. FT-IR spectra of the synthesized photocatalysts.

3.2. Specific surface areas

The specific surface areas (SSAs) of fine particles are shown in Table 2. SSA has been confirmed to have considerable impacts on cement hydration [51], formation of hydration products [52], and photocatalytic efficiency [53,54]. For example, nanosilica with a higher SSA is involved in cement hydration with a higher priority than microsilica with a smaller SSA [55,56]. Hence, it is reasonable to assume that particles with different SSAs would influence the physicochemical changes upon hydration and carbonation, as well as the self-cleaning property [57].

3.3. Porosity & pore size distribution

The self-cleaning property of PCBMs is dependent on the microstructure, phase composition, phase distribution, and optical properties. All mortar samples are fully penetrated by CO_2 after the 28d accelerated carbonation as shown in Fig. S2. Samples without the accelerated carbonation are labeled as "NC", and samples with accelerated carbonation are labeled as "AC".

Pores in cementitious materials are generally classified into four categories: gel pores (<10 nm), medium capillary pores (10–50 nm), large capillary pores (50 nm-1 μm), and macropores and entrained air pores (>1 μm) [52]. Before carbonation, the gel and capillary pores were refined with hydration as shown in Fig. S3a [36,43]. The pore volume of the Sa at the 30–300 μm range is lower than the Cp after 7d hydration, attributed to the "filler" effect of microsilica. From 7d to 28d, more C-S-H gel is generated from the pozzolanic reaction of microsilica with solid volume expansion, which refines the pore structure [83]. Porosities of all samples decrease but average pore diameters get coarser after carbonation. This is attributed to the depletion of gel and capillary pores upon carbonation as shown in Fig. S3b.

Surfactant Triton X-405 as a typical foaming agent would introduce air bubbles into the cementitious matrix. It is proved that surfactant-induced pores in the mortar matrix are generally bigger than 150 μm, which mainly affects the macrostructure [37]. Porosity increase in Cp is observed from 7d to 28d hydration which might be attributed to 1) the slight randomness of macropore numbers and 2) the considerable impact of macropores (pore radius, r) on the pore volume and porosity ($V = 4/3\pi r^4$) (Table 3).

The pore size distribution of all PCBMs changes in the 4–100 nm range (see Fig. 3a). An overall tiny decrease of pore volume in Cp (cement+P25) is observed, while the pore volume increases in the <7 nm range and decreases in the 7–100 nm range in Sa (cement+microsilica+AT). The pore volume of Ca (cement+AT) shows a linear assembly of Cp and Sa, due to the existence of silica aerogel. Gel and capillary pores in pure cement mortar slightly change, while more gel pores are generated with fewer capillary pores thanks to the pozzolanic reaction of microsilica, with the hydration from 7d to 28d. It is found upon carbonation in Fig. 3b: 1) the pore volume decreases at both gel and capillary scales, 2) the smaller the pore diameter, the more dramatic the pore volume decrease, and 3) the higher the reactive silica content, the higher the decreased extent. It is caused by different C-S-H contents after 28d hydration.

Generally, the addition of nanoparticles can refine the pore structure [60,61]. It is proved that, after 28d hydration, the 5 wt% of TiO_2 addition can refine the pore structure in all diameter ranges, while the 1 wt% of TiO_2 addition can only refine the pore structure in the >100 nm range [60]. That indicates the refinement of pore structure in <100 nm range of AT- and ST- blended samples (1 wt% TiO_2) is mostly attributed to the "photocatalyst silica" and microsilica (if used).

Table 2
The specific surface area of powders.

Material	$NanoSiO_2$	SiO_2 aerogel	ST	AT	P25	Microsilica
SSA [m^2/g]	275.8 ± 13.8	715.9 ± 43.3	199.6 ± 11.6	482.9 ± 3.7	50 ± 15[a]	20 ± 10[a]

[a] Provided by the manufacturer (BET method).

3.4. Phase composition

The self-cleaning property of PCBMs is affected by the effective exposure of TiO_2 particles on the surface, while the hydration and carbonation products could shield TiO_2 particles and alter the properties of the surrounding media. To observe the phase evolution upon hydration and carbonation, XRD, TGA, and SEM analyses are utilized to characterize the phase composition.

Similar mineral composition and hydration products are observed in uncarbonated mortars (Fig. 4a): 1) several peaks dominated by quartz ascribing to the sand, 2) main cement clinkers including C_2S, C_3S, and C_3A, 3) main crystallized hydrates including CH and AFt, and 4) TiO_2 in all samples [12,16]. The CH content ($2\theta = 20.96°$) is almost unchanged in the hybrid group with the increase in hydration age, while the increased amount of CH is observed in the control group. Similar results are also reported in other studies [11,41,42]. Similar composition and carbonation products are observed in the carbonated mortars (Fig. 4b): 1) the peak intensity of calcite ($2\theta = 34.24°$) of the control group is stronger than in the hybrid group, 2) CH and cement clinkers (C_2S and C_3S) are almost invisible due to carbonation. From these results, it is concluded that there is no vaterite and aragonite after the 28d accelerated carbonation.

TGA data are analyzed to further study the phase composition of PCBMs with different treatments. DTG curves in Fig. 5 show temperature ranges of mass loss for mortars before and after carbonation. The amorphous calcium carbonate in uncarbonated samples is attributed to the inevitable CO_2 exposure of the sample surface during the mixing, casting, and characterizations. The mass loss in the 400–800 °C range corresponds to the decarbonization of calcium carbonates for carbonated samples [11,39,62–64]. Thermal decomposition temperatures of amorphous $CaCO_3$ and calcite overlap in a broad range, but amorphous $CaCO_3$ decomposes at a lower temperature [11,39,65,66]. Therefore, the 400–650 °C range is assigned to the decomposition of amorphous $CaCO_3$, while 650–800 °C is assigned to calcite, based on the DTG curves. More mass loss of amorphous $CaCO_3$ in the hybrid group and more mass loss of calcite in the control group are observed, caused by different C-S-H content before carbonation (Fig. 5b). Meanwhile, more amorphous $CaCO_3$ is observed in hybrid samples with the increase in hydration age, which is attributed to the increased C-S-H content in hybrid samples upon hydration. It means that the addition of reactive silica and age of carbonation considerably influence the phase composition upon carbonation, owing to the different carbonation behaviors of hydration products and cement clinkers.

The stochastic uncertainty of TGA tests for mortar samples has been discussed due to the use of sand use [65,67]. A mass loss-based normalization that can semi-quantitatively determine the mass loss of certain phases with certain mass loss temperature ranges is adopted [65]. The normalized mass loss of a certain phase is calculated by:

$$m_{nor,x} = (m_{x.1} - m_{x.2})/m_t \times 100\% \quad (2)$$

where, $m_{nor,x}$ is the normalized mass loss of phase x [%], $m_{x.1}$ is the mass ratio of the sample at the temperature when phase x starts the decomposition obtained from the TGA curve [%], $m_{x.2}$ is the mass ratio of the sample at the temperature when phase x ends the decomposition obtained from the TGA curve [%], m_t is the total mass loss ratio of the sample for the whole heating process obtained from the TGA curve [%].

The normalized mass loss (CH of uncarbonated samples and calcite of carbonated samples) is calculated and summarized in Table 4. The calculation is based on the decomposition temperature ranges

Table 3
Changes of microstructure upon hydration and carbonation.

Condition	Sample	Porosity [%]	Total pore volume (V) [ml/g]	Total pore area (A) [m^2/g]	Average pore diameter (4 V/A) [nm]
Hydration	Cp-7d-NC	24.82	0.1368	7.910	69.19
	Ca-7d-NC	30.28	0.1780	8.107	87.83
	Sa-7d-NC	29.46	0.1785	13.983	51.07
Carbonation	Cp-28d-NC	27.67	0.1198	2.088	88.76
	Ca-28d-NC	29.89	0.1445	2.851	80.62
	Sa-28d-NC	24.27	0.1290	4.474	47.12
	Cp-28d-AC	23.27	0.1566	7.056	229.55
	Ca-28d-AC	25.69	0.1755	8.705	202.79
	Sa-28d-AC	23.44	0.1400	11.883	115.36

Note: the MIP profiles of the accumulative pore volume are included in Supplementary Materials (Fig. S4).

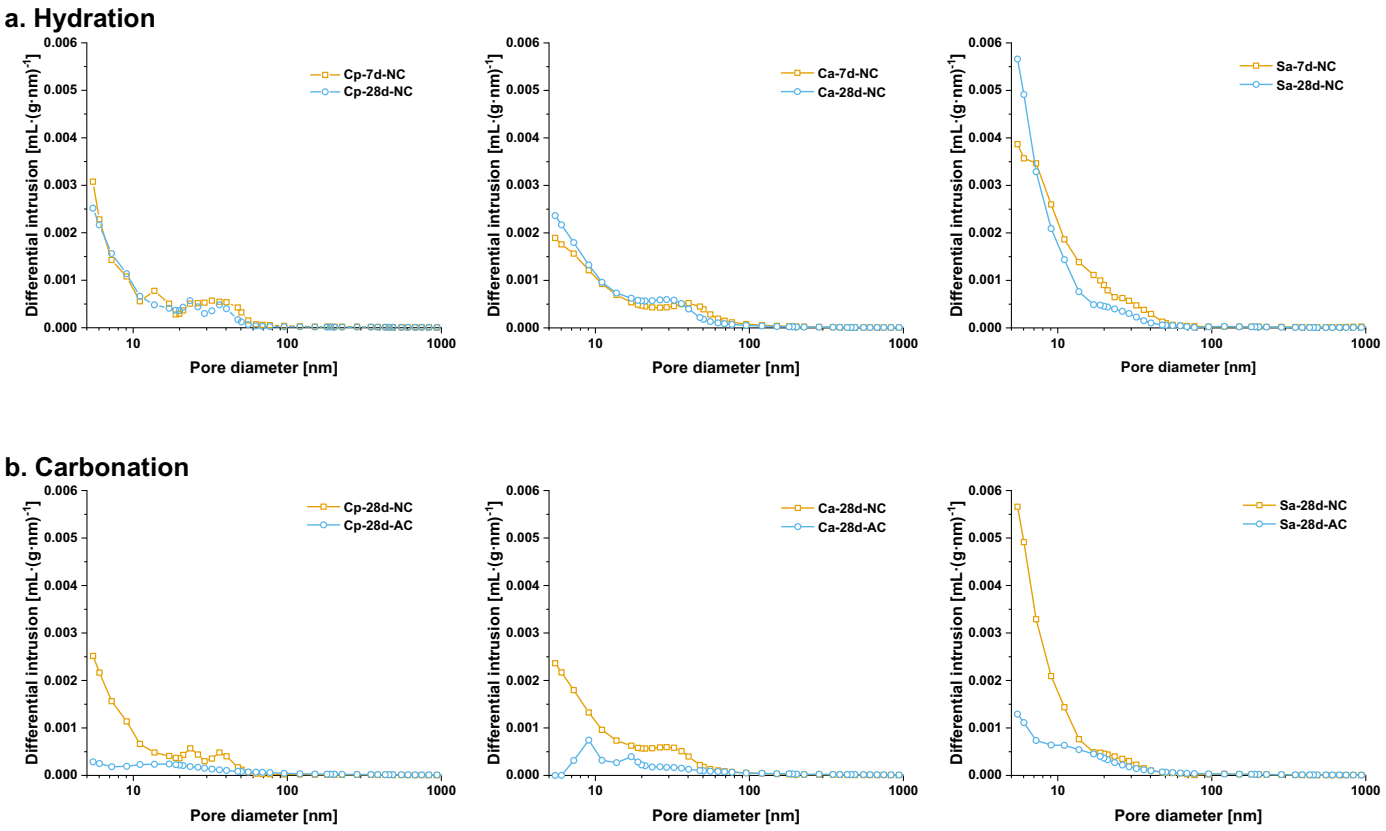

Fig. 3. The differential pore size distribution upon (a) hydration and (b) carbonation of PCBMs.

determined by DTG curves. CH is accumulated in the control group (cement + photocatalyst) with the increase in hydration age, which is in line with XRD results. Meanwhile, a lower content of CH in samples with composite photocatalysts is observed compared with P25-addition samples and is more visible in AT-blended samples. It confirms the involvement of nanosilica and silica aerogel in the pozzolanic reaction as described in Section 3.2.1. The reactivity of the three reactive silicas is ordered as: silica aerogel > nanosilica > microsilica. More TiO_2 particles (of AT- and ST-blended samples) are then "encapsulated" with porous C-S-H gel due to in-situ pozzolanic reaction of nano silica and silica aerogel, with the increase in hydration age. Calcite, poorly crystalline C-S-H, and amorphous $CaCO_3$ are the main carbonates according to Table S1, Table S2, and Fig. 6b. More amorphous $CaCO_3$ is generated when C-S-H with a low Ca/Si ratio is carbonated as expected.

Fig. 6 shows the SEM images of the 28d-hydrated Cp and Sp before and after carbonation. Before carbonation, rich crystallized phases (AFt and CH) and less C-S-H gel are observed in Cp, while compact C-S-H gel and less crystallized CH are observed in Sp. Upon carbonation, dense "flaky-shaped" and "cluster-shaped" crystallized phase (calcite) and porous C-S-H gel are observed in both Cp and Sp, while the C-S-H gel in Sp with microsilica is more porous [11,68]. C-S-H gels turn to be more porous with a lower Ca/Si ratio after carbonation due to the "decalcification" [68]. These observations are in line with the analyses of phase composition by XRD and TGA.

3.5. Optical properties

UV-VIS-NIR reflection spectra of PCBMs before and after carbonation are measured. The band energy (E_g) is calculated from spectra, based on Tauc's plot method [69]. The Kubelka-Munk optical absorption coefficient $F[R(\lambda)]$ is first calculated by:

$$F[R(\lambda)] = [1 - R(\lambda)]/2R(\lambda) \quad (3)$$

then, E_g is obtained by (Tacu's plot):

$$F[R(\lambda)]h\upsilon = \left(h\upsilon - E_g\right)^n \quad (4)$$

where, $R(\lambda)$ is the reflectance of the mortar plate [%], n is the constant

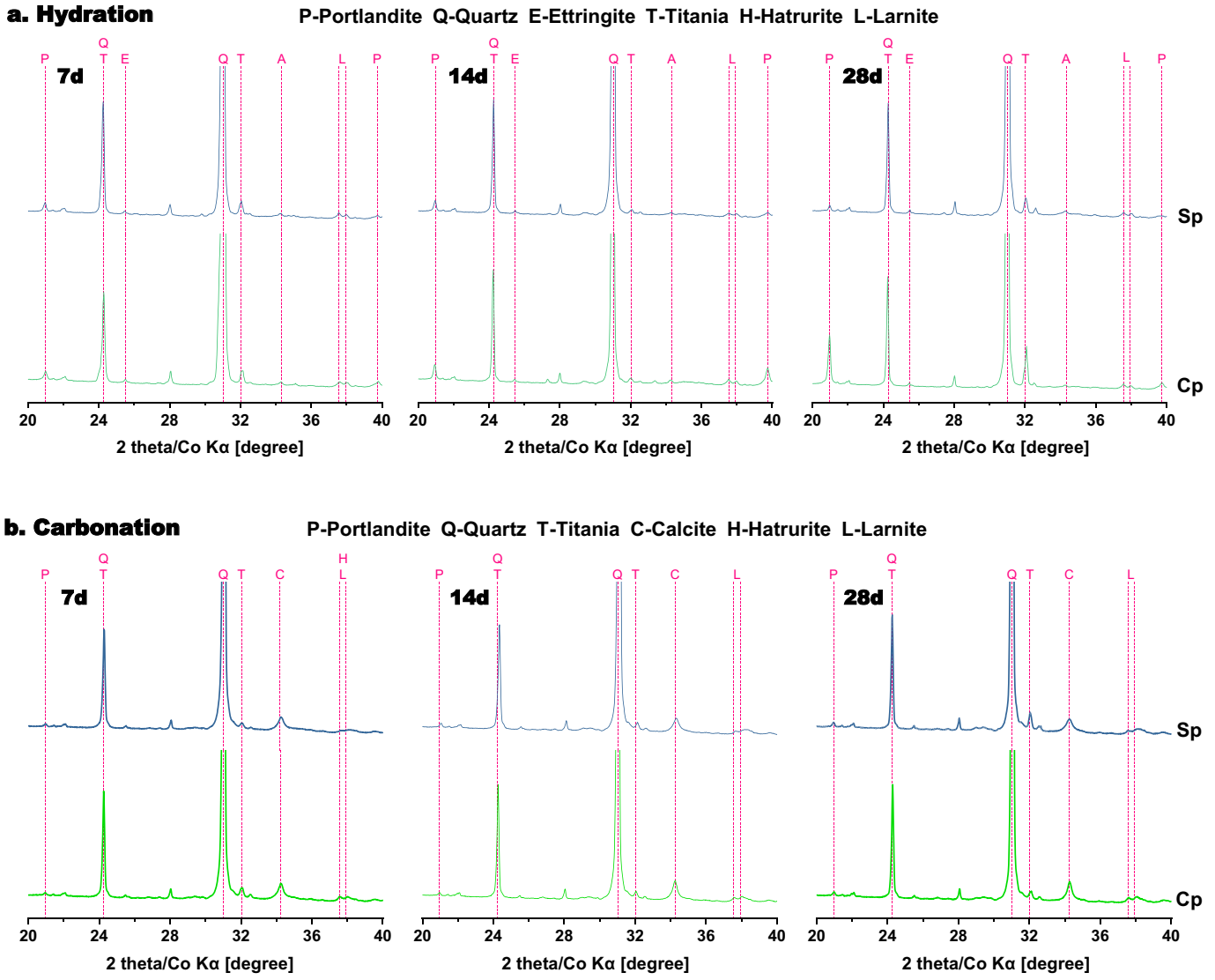

Fig. 4. XRD patterns of PCBMs (a) before and (b) after carbonation.

that depends on the type of transition (2 for indirect transition, 1/2 for direct transition), h is the Planck constant (6.63×10^{-34} J·s), υ is the photon's frequency [1/s]. For TiO_2-contained compounds, indirect transition ($n = 2$) is generally considered and discussed [70–72].

The activation of photocatalysts is related to the UV absorption capacity [73]. For non-transparent objects like cementitious mortars, the UV absorptance can be obtained based on the reflection spectrum (absorptance = 1-reflectance). A higher UV absorptance indicates a stronger UV absorption capacity. To compare the UV absorption capacity of different PCBMs, the average UV absorptance (ρ_{UV}) of each sample in the 250–400 nm band is defined and calculated by:

$$\rho_{UV} = \frac{\sum_{m_1}^{m} 1 - R(\lambda)_m}{m} \tag{5}$$

where, λ is the wavelength [nm], $R(\lambda)$ is the reflectance, m is the count of the reflection spectrum measurement at the UV range.

It is found in Fig. 7: 1) carbonation causes more drop in the UV absorption capacity than hydration, 2) P25-blended samples have the highest UV absorption capacity and show better resistance to the deterioration upon carbonation/hydration than composite photocatalysts-blended samples, 3) samples with the microsilica addition show better resistance against the deterioration caused by carbonation than samples using pure cement as the binder, and 4) the composite photocatalyst with silica aerogel shows better resistance against the deterioration caused by carbonation/hydration than the nanosilica one. These results indicate the dosage of TiO_2 (5 %/1 %), binder mix (cement/cement+microsilica), and composition of synthesized photocatalyst (silica aerogel+TiO_2/nanosilica+TiO_2) affect the deterioration of UV absorption capacity upon carbonation and hydration. A higher dosage (5 %) of TiO_2, the substitution of cement with microsilica, and silica aerogel composited photocatalyst can improve the resistance to the deterioration of UV absorption capacity upon hydration and carbonation. It must be borne in mind that the change of matrix color upon hydration/carbonation could also alter the UV absorption capacity of PCBMs to some extent, according to "Planck's blackbody radiation law" [74]. However, the change in UV absorption should be mainly attributed to the photon transition of TiO_2 particles, because of the sheltering of hydration/carbonation products on TiO_2 surfaces.

Band energies of photocatalyst-blended mortars are calculated and summarized in Fig. 8. The band energy of PCBMs (2.83–3.04 eV) is lower than TiO_2 (~3.2 eV), which was observed in other studies [12,75]. The reduction of band energy is attributed to the disorder of the electronic structure of semiconductors through the creation of defects [12,76]. However, the defects (surface modification) do not always

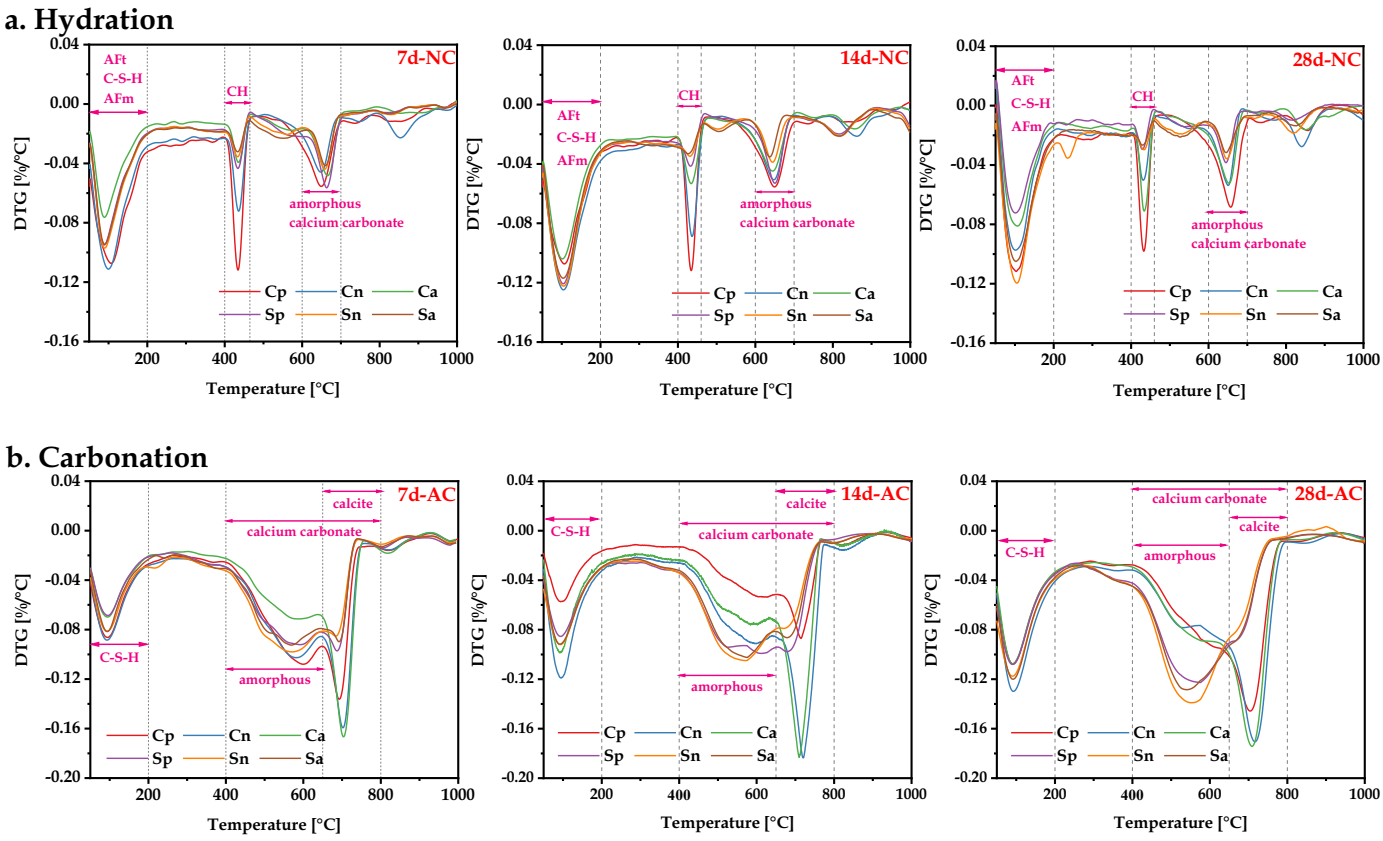

Fig. 5. DTG curves of PCBMs (a) before and (b) after carbonation.

Table 4
Normalized mass loss of CH before carbonation and calcite after carbonation.

Sample	Normalized mass loss of CH [%]			Normalized mass loss of calcite [%]		
	7d	14d	28d	7d	14d	28d
Cp	9.93 ± 0.05	11.34 ± 0.11	13.53 ± 0.19	28.21 ± 0.93	35.21 ± 0.03	36.05 ± 0.18
Cn	8.35 ± 0.11	9.44 ± 0.18	10.51 ± 0.08	25.84 ± 0.08	31.97 ± 0.11	31.55 ± 0.11
Ca	7.29 ± 0.25	8.01 ± 0.28	8.91 ± 0.08	24.93 ± 0.40	31.64 ± 0.63	31.17 ± 0.08
Sp	6.72 ± 0.14	5.49 ± 0.09	4.99 ± 0.06	18.91 ± 0.03	19.86 ± 0.06	13.69 ± 0.18
Sn	5.42 ± 0.04	4.06 ± 0.07	4.00 ± 0.04	16.24 ± 0.09	16.58 ± 0.08	12.34 ± 0.16
Sa	5.04 ± 0.04	3.80 ± 0.02	3.75 ± 0.10	15.52 ± 0.06	15.84 ± 0.17	12.43 ± 0.06

Note: $m_{x,1}$ and $m_{x,2}$ are 400 °C and 465 °C for CH, 650 °C and 800 °C for calcite.

guarantee the drop of band energy [77,78]. The accumulation of hydration/carbonation products might bring higher band energy. The increase in band energies by hydration/carbonation indicates fewer photons (less energy) can be utilized in photocatalysis after hydration and carbonation. The band energy of PCBMs increases differently upon hydration (ages) and carbonation: 1) the band energy is more sensitive to hydration than carbonation, 2) the band energy of the control group is more sensitive to hydration/carbonation than the hybrid group, and 3) the band energy of ST-addition (nanosilica+TiO_2) is more sensitive to hydration/carbonation than AT-addition (silica aerogel+TiO_2) samples within groups. The higher band energy indicates higher energy (of photons) to trigger the photocatalytic reaction. Therefore, the increase of band energy means the deterioration of the photocatalytic property when photocatalysts are applied in buildings. Some studies were conducted to investigate the band energy of photocatalytic cementitious materials [14,20,35,77]. However, most of them focused only on the impact of catalysts, while the impact of hydration, especially carbonation was ignored. The increase of band energy could be attributed to the (over-) surface modification of TiO_2 particles by nano-sized hydration/carbonation products as electronic impurities [12,77]. These results reveal that the nano-sized hydrated/carbonated impurities might destruct the electronic structure, drift conduction/valance bands, and disturb the light absorption and charge separation of (modified-) TiO_2 particles [77,78]. It could be concluded that crystalized phases (mainly CH and calcite) affect more the semiconductor properties than amorphous phases (mainly C-S-H) in PCBMs, which might be ascribed to the more stable and consistent optical properties and electronic structure of crystallized phases than the amorphous ones [79].

3.6. Discoloration process

RhB on the surface will be degraded by the photocatalytic reaction with the UV exposure, as presented in Fig. 9. There are three stages of the discoloration process visibly identified as: 1) active stage with rapid color change, 2) transitional stage with slight color change, and 3) stable stage with almost no color change. Most dye should be oxidized in the active stage to prevent the accumulation of pollutants on the surface. The accumulated pollutants would cover the photocatalyst surface and then retard further degradation if a sustained pollution source exists. In recent studies of photocatalytic cementitious materials, there is no clear definition of the active stage, but it should be imperative based on the analysis above [12]. The discoloration process of different samples is similar, and a^* of all samples is relatively stable after 345 min UV irradiation (Fig. 9 and Fig. S7). Meanwhile, different final color changes are observed at the stable stage after long-time UV irradiation, which means partial RhB could not be oxidized by the photocatalytic reaction. Therefore, $\varphi_{t=105\ min}$ and $\varphi_{t=2800\ min}$ are utilized as indicators to better

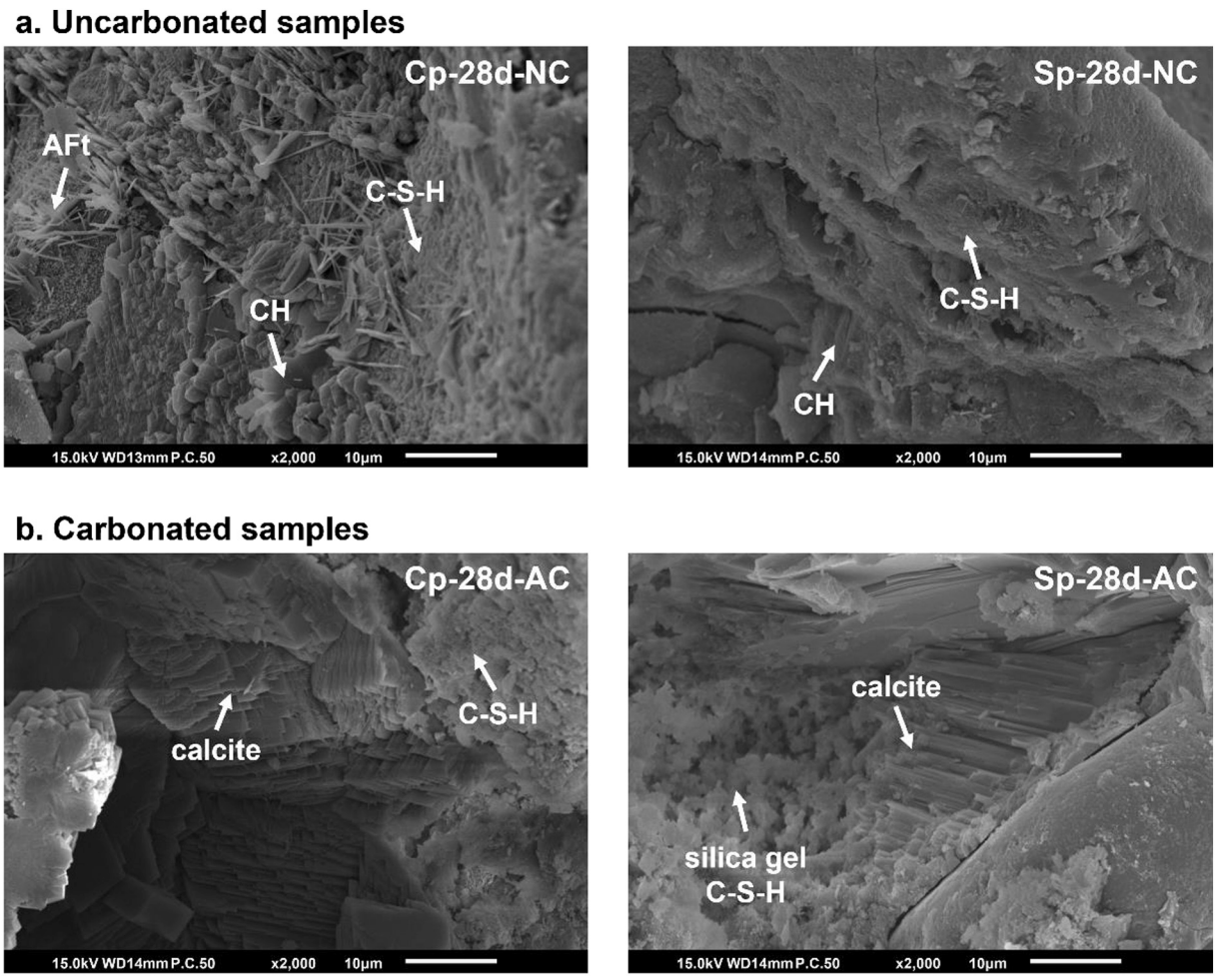

Fig. 6. SEM images of (a) uncarbonated and (b) carbonated PCBMs.

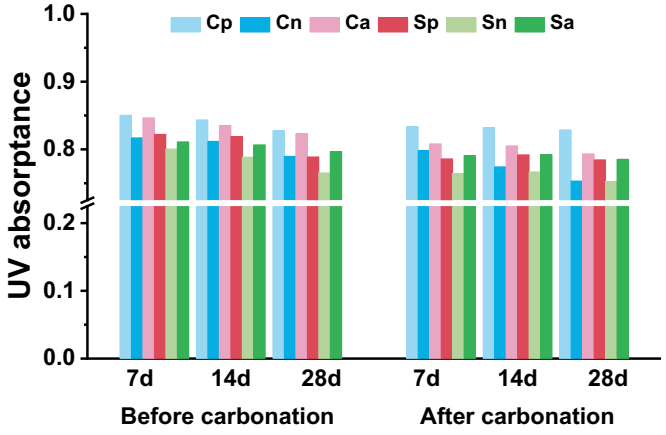

Fig. 7. Average UV absorptance (λ ~ 250–400 nm) of PCBMs before carbonation and after carbonation.

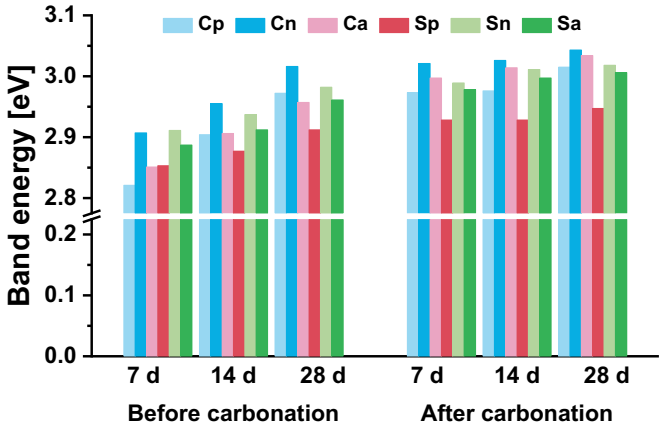

Fig. 8. Band energy of PCBMs before carbonation and after carbonation.

compare the self-cleaning efficiency for the active stage and final discoloration performance, as concluded in Fig. 10.

Overall decreases and similar variations at $\varphi_{t=105\ min}$ and $\varphi_{t=2800\ min}$ are both observed upon hydration and carbonation in Fig. 10. This indicates both hydration and carbonation harm the discoloration efficiency of the active stage and the final discoloration rate. In detail, the performance drops with the increase of hydration age prior to carbonation. The differences between samples become smaller after carbonation. Meanwhile, samples of the hybrid group (cement+microsilica) show better resistance to the deterioration of self-cleaning performance (both active and stable stages) caused by hydration/carbonation than samples of the control group. At the same time, P25-blended samples always demonstrate the best performance, while AT-blended samples perform better than ST-blended samples. These results are in line with the observation of the optical property.

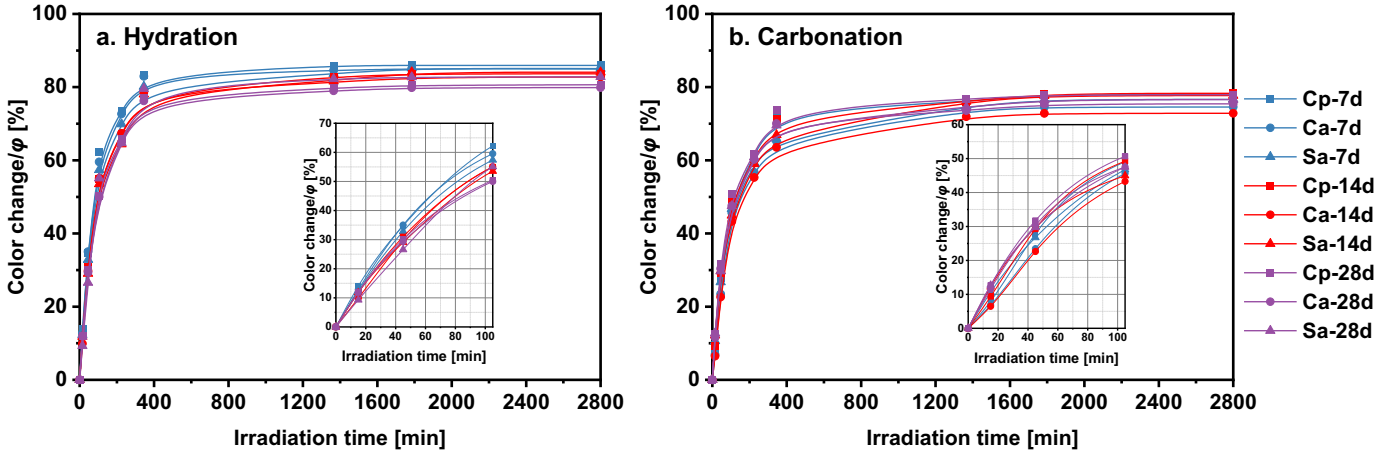

Fig. 9. Discoloration process of (a) uncarbonated and (b) carbonated PCBMs with UV irradiation.

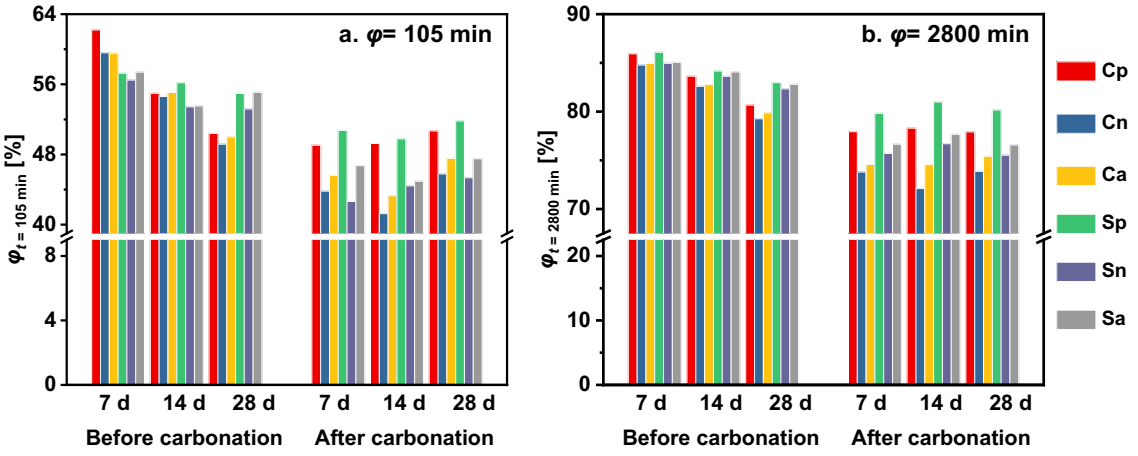

Fig. 10. Color change of uncarbonated and carbonated PCBMs for the (a) active stage and (b) stable stage.

4. Discussions

The self-cleaning property of PCBMs will be debilitated by hydration and carbonation according to the analyses in Section 3. The "occupation" of active sites by nano-sized hydration/carbonation products at the early stage and the "sheltering" effect of hydration/carbonation products are difficult to interpret, especially when SCMs are utilized. For example, in this study, the self-cleaning performance of AT-blended samples is expected to be the worst based on these theories due to the high specific surface area of AT, but it is in contrast with the experimental observation. Hence, new mechanisms are proposed in this study to better demonstrate the deterioration of the self-cleaning property caused by hydration and carbonation.

The increase of band energy and the decrease of UV absorption capacity are attributed to the surface modification of TiO_2 particles by the nano-sized hydration/carbonation products in Section 3.5. Initial variables between samples in this study are the reactive silica and the dosage of TiO_2. It is easy to understand that a matrix with a higher dosage (5 %) of TiO_2 can perform better than the one with a smaller dosage (1 %), because of the higher initial exposure of TiO_2 and the "dilution" effect on the negative impacts when TiO_2 particles are well dispersed. So, discussions will mainly be focused on hydration/carbonation products, photocatalyst properties, and surrounding media. These properties are affected by reactive silica (microsilica, photocatalyst@nanosilica, photocatalyst@silica aerogel).

4.1. Deterioration mechanism of self-cleaning performance upon hydration

More CH crystals and high Ca/Si C-S-H gels are generated and adhered to the photocatalyst surface, with a higher pH environment around photocatalyst particles in OPC-based matrixes [80,81]. Meanwhile, the pH is lower with the (increased) SCMs addition and could decrease to <13 for the blends with high silica fume substitution (>20 wt%) [82–85]. The surrounding media of TiO_2 particles are C-S-H and CH for control samples (28d) and low Ca/Si C-S-H for hybrid samples (28d) before carbonation (Section 3). After carbonation, the surrounding media for TiO_2 particles are low Ca/Si C-S-H and calcite for control samples (28d) and low C-S-H, silica gel, and amorphous $CaCO_3$ for hybrid samples (28d). However, these phases possess different mass transfer capacities which could affect the photocatalytic reaction [12,86]. For example, calcite is denser than amorphous calcium carbonate, which limits the mass transfer and then the photocatalytic performance. Meanwhile, the oxidization of H_2O_2 to OH· and OH^- will be retarded if rich OH^- exists considering the kinetic balance [87]. This indicates the high pH also contributes to the drop in photocatalytic activity from the perspective of chemical equilibrium. In addition, the microstructure of the surrounding media concerning the mass transfer of pollutants also affects the photocatalytic efficiency [9,46].

The gel structure of C-S-H is the dominant factor affecting the micro-mass transfer for photocatalytic oxidation. More low Ca/Si C-S-H is formed to replace the CH which is originally adhered to the photocatalyst surface when reactive silica exists, leading to the formation of

more gel pores and the drop in pH around TiO_2 particles. Low Ca/Si C-S-H is much more porous than the crystallized CH, which allows a better mass transfer and alleviates the deterioration of self-cleaning performance [88]. The above discussion can explain why samples with microsilica show higher resistance to the deterioration of self-cleaning performance than samples using pure OPC.

The pozzolanic reaction occurs preferentially with nanosilica and silica aerogel, attributing to their high SSAs, for samples using composite photocatalysts. The "TiO_2@SiO_2 Core-Shell" structure of AT and ST is further reconstructed as TiO_2 particles and TiO_2-surrounded C-S-H. The gel structure of AT-contained samples is more porous than ST-contained samples, attributed to the intrinsic porous frame structure of silica aerogel. This indicates a better resistance to the deterioration of self-cleaning performance upon hydration, which is in line with the observation in Section 3.3. The deterioration mechanism of self-cleaning performance by hydration and carbonation is summarized in Fig. 11 and further explained in the following sections.

Fig. 12a shows the changes of photocatalysts and their surrounding conditions of different initial compositions upon hydration. The deterioration of PCBMs is attributed to four factors: 1) band energy (nano-sized surface modification), 2) "sheltering" effect, 3) chemical equilibrium, and 4) gel mass transfer. The alleviation effects of microsilica and "photocatalyst@silica" can be explained by these factors. Three groups are plotted in Fig. 12b for a better expression: I. Cement + P25, II. Cement + MS + P25, and III. Cement + MS + AT. With the increase of reactive silica content (0 → 25 % wt% MS → 25 % wt% MS + 4 wt% photocatalyst@silica), the deterioration of self-cleaning performance is retarded.

At the 7d age:

- the pH, CH content, and Ca/Si (of C-S-H) of the OPC-based matrix are the highest among the three groups, which indicates the highest OH^- concentration, strongest "sheltering" effect/surface modification, and worst gel mass transfer.
- with the substitution of microsilica (25 wt%), the pH and Ca/Si become lower, and more C-S-H gels with more porous structure are produced, which indicates lower OH^- concentration, less "sheltering" effect/surface modification, and better gel mass transfer.
- the photocatalyst@silica is preferentially transferred as the porous "photocatalyst@CSH" (low Ca/Si) when AT photocatalyst is used with microsilica (25 wt%). This indicates the lowest OH^- concentration, further reduced "sheltering" effect/surface modification, and further enhanced gel mass transfer.

With the increase in hydration age (7d → 28d):

- all matrixes are surrounded by more hydrates with the enhanced "sheltering" effect and surface modification.
- the pH becomes lower and more C-S-H gels (more porous) exist for groups II and III, which indicates the lower OH^- concentration and better mass transfer that can alleviate the deterioration of photocatalytic properties to a certain extent.
- the pH becomes higher in group I, which indicates higher OH^- concentration and results in a worsened deterioration.

4.2. Deterioration mechanism of self-cleaning performance upon carbonation

Calcium carbonates (amorphous and calcite) are produced from the carbonation of cement grains and hydrates upon carbonation. CH is generally transformed to calcite with solid volume increase, while C-S-H is partially carbonated as calcite and C-S-H (lower Ca/Si), according to Section 3.2.1. An overall stronger "sheltering" effect is formed after a 28d CO_2 treatment (3 %) in all samples as shown in Fig. 13. The matrix is more pH neutral after carbonation, indicating the changed mass transfer and chemical equilibrium of the surrounding media. More calcite crystals could further modify the optical properties of TiO_2 particles [79]. Hence, the enhanced "sheltering" effect, gel structure refinement (worse mass transfer), and retarded photocatalytic reaction result in lower photocatalytic activity. It manifests as the increment of band energy, drop of UV absorption, and deterioration of self-cleaning performance upon carbonation.

Less calcite is generated in samples with microsilica, while more amorphous calcium carbonates are generated especially visible for 28d samples, due to the massive production of C-S-H (Table 4). Carbonation products of C-S-H gel are low Ca/Si C-S-H gel, silica gel, and amorphous calcium carbonate (partially as calcite). From SEM observations, the gel structure is more porous even though the volume of gel pores decreases, which could alleviate the deterioration of mass transfer. Meanwhile, more low Ca/Si C-S-H gels are retained in hybrid samples after carbonation, due to the thermodynamic priority of high Ca/Si C-S-H and the lower limit of Ca/Si ratio for the "decalcification" process [89,90].

Besides, the "TiO_2@C-S-H Core-Shell" structure is reconstructed by carbonation. The photocatalyst@C-S-H would be carbonated to multi-phase (C-S-H gel, silica gel, and calcium carbonates [91]. The microstructure of the new photocatalyst@C-S-H is more porous than the carbonated C-S-H of hybrid samples with P25 addition. Affecting factors (surface modification, sheltering effect, gel mass transfer, and chemical equilibrium) upon carbonation, originally caused by microsilica and photocatalyst@silica are summarized and presented in Fig. 13c.

4.3. Interaction of hydration & carbonation

The impact of hydrates carbonation at different hydration ages is systematically discussed above. Therefore, only anhydrous cement phases are considered in this section. Carbonation takes the kinetic

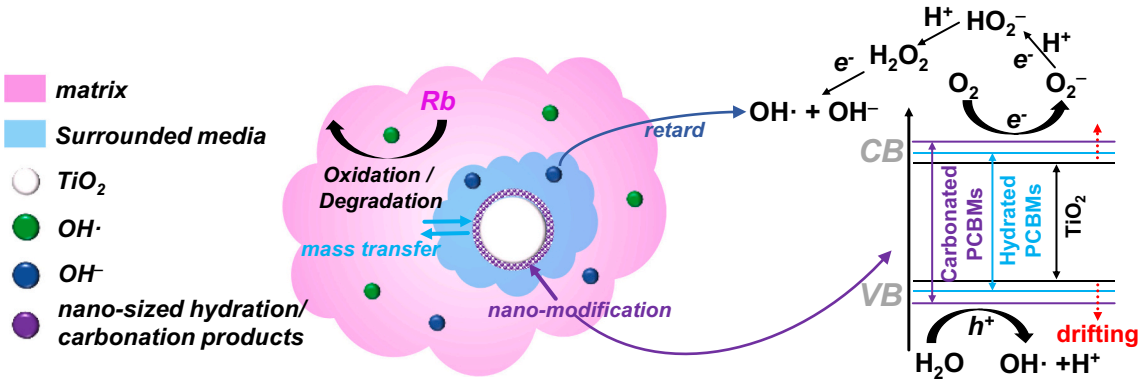

Fig. 11. The deterioration mechanism of self-cleaning performance of PCBMs.

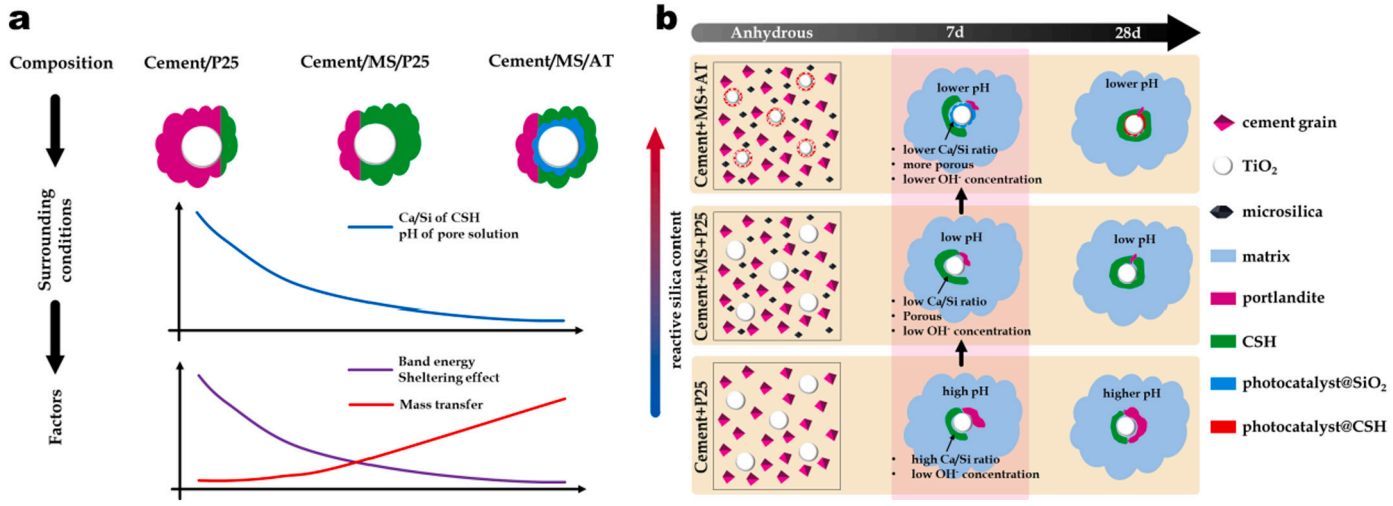

Fig. 12. Deterioration mechanism of self-cleaning performance and the alleviation effects of microsilica and "TiO_2@SiO_2 Core-Shell" photocatalysts upon hydration (a. logical diagram and b. schematic).

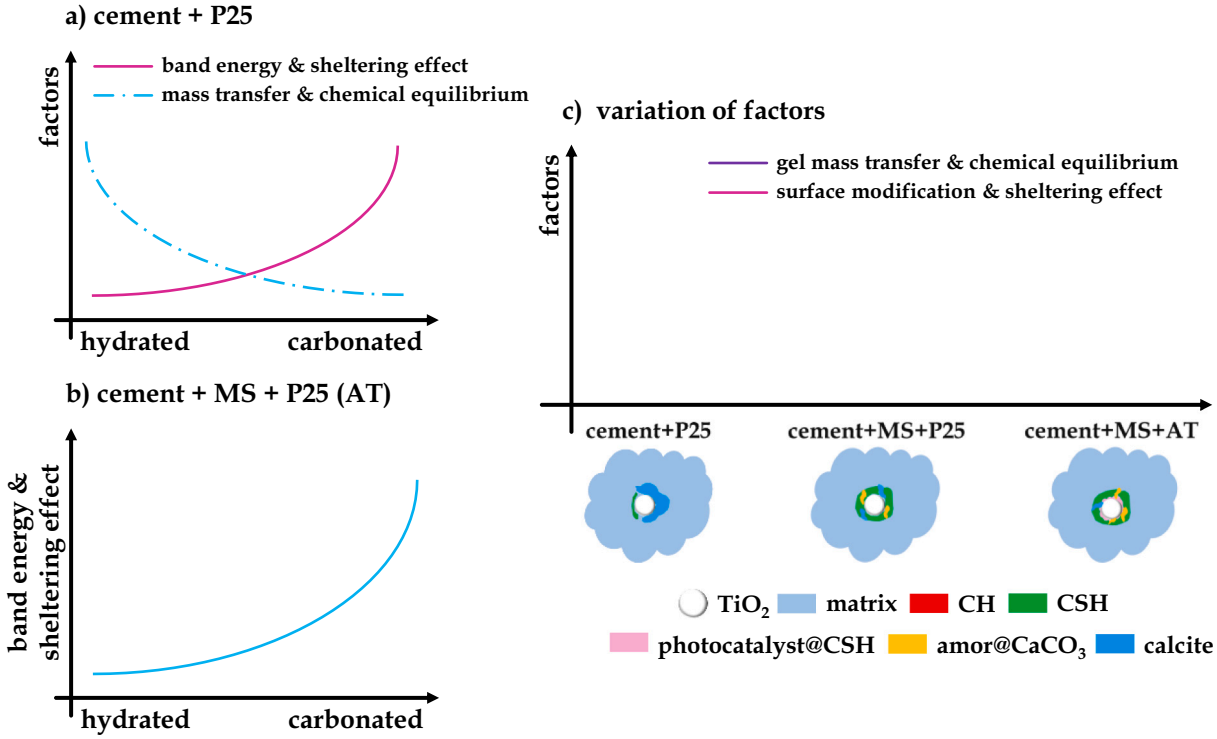

Fig. 13. The variation of the four factors affects the self-cleaning performance of different PCBMs upon carbonation.

priority over hydration and the stable carbonation products are mainly calcite (partially as C-S-H), gibbsite, silica gel, and $Fe(OH)_3$, for anhydrous cement grains (e.g. C_3S, C_2S, C_3A, and C_4AF) in a humid CO_2-riched environment [14,15,92,93]. This is also validated by the TGA results (Fig. 5b and Table 4), while more calcite is observed in hybrid samples upon carbonation after 7d and 14d hydration than 28d. Then, the optical and self-cleaning properties are altered, as presented in Sections 3.5 and 3.6. Therefore, the early carbonation (7d and 14d) might exacerbate the deterioration of self-cleaning properties as shown in Figs. 9b and 10, which could be attributed to the decrease of C-S-H content (weakened gel mass transfer and stronger "sheltering" effect). Generally, the carbonation of cementitious materials is treated as a diffusion-controlled process, and the CO_2 partial pressure of the accelerated carbonation (3 %) is about 100 times of the natural process (0.03 %), which indicates a much slower CO_2 penetration and carbonation speed in nature [15,39,94]. However, self-cleaning is a surface property, and the mortar surface is quite easy to be naturally carbonated with the appearance of amorphous $CaCO_3$ and then calcite (the early carbonation product of CH [15]) as shown in Fig. 5a. Therefore, the negative effect of early natural carbonation could be also alleviated by utilizing reactive silica in the application, to promote the instantaneous secondary hydration of CH [68].

4.4. Solution and further works

The substitution of cement with microsilica is proved to be an

efficient approach against the deterioration of self-cleaning performance caused by hydration and carbonation, which is concluded as "matrix resistance". The "TiO_2@SiO_2 Core-Shell" structure can further prevent the drop in self-cleaning performance, which is concluded as the "intrinsic resistance" of composite photocatalysts. Taking all the analysis and discussion into consideration, an appropriate solution should consider: 1) a sufficient net TiO_2 dosage, 2) a hybrid binder (cement + reactive silica) design, and 3) a (pseudo) "core-shell" structure of photocatalyst by using fine reactive silica (for example silica aerogel) as the support.

It should be noted that the mechanical property and erosion resistance of cementitious materials are also of considerable significance for engineering applications. The overdose of microsilica would harm the mechanical property and erosion resistance capacity in long-term service, as well as cause cost issues [41,62,66]. So an optimal dosage of reactive silica is necessary to ensure simultaneously sufficient self-cleaning performance, mechanical property, and erosion resistance. At the same time, the property like core/shell ratio (mass and thickness) and shell porosity of the "TiO_2@SiO_2 Core-Shell" photocatalyst is also worth further investigation.

5. Conclusions

This study attempts to understand the deterioration mechanism of photocatalytic cementitious materials upon simultaneous hydration and carbonation. Two series of photocatalytic mortars using two binders and three photocatalysts are fabricated, characterized, and analyzed to identify the evolution of phase composition, microstructure, optical properties, and self-cleaning performance. The detailed conclusions are drawn as follows:

1. Deterioration mechanisms of self-cleaning performance upon hydration and carbonation, concerning properties of photocatalysts (UV absorption, band energy, "sheltering" effect of TiO_2 particles) and their surrounding media (gel mass transfer and chemical equilibrium), are proposed.
2. The increased band energy is ascribed to the surface nano-modification of hydration/carbonation products, with the drifting of conduction/valance bands of TiO_2 particles. Crystallized phases (CH and calcite) with more stable and consistent optical properties and electronic structure could have a stronger modification capacity than the amorphous ones. A stronger "sheltering" effect is attributed to the accumulation of hydration/carbonation products, especially the crystallized phases (mainly portlandite and calcite) with compact structures. The worsened gel mass transfer property is caused by the reduction of gel pores. The chemical equilibrium of photocatalytic reaction is affected by pH (OH^- concentration) and a low pH is beneficial.
3. More low Ca/Si and porous C-S-H gels are generated with microsilica substitution due to the pozzolanic reaction. This results in the enhanced resistance to the deterioration of self-cleaning performance on hydration, reflected by lower band energy, weaker "sheltering", better mass transfer, and lower pH compared to OPC-based samples.
4. Low Ca/Si "photocatalyst@C-S-H" with a more porous structure could be preferentially formed by the in-situ pozzolanic reaction of "photocatalyst@silica" around TiO_2 particles owing to the high SSA. The porous "photocatalyst@C-S-H" could limit surface modification and "sheltering" effect, enhancing the gel mass transfer. The extra reduction of OH^- concentration could promote the chemical equilibrium as well.
5. The "sheltering" effect becomes more evident in all matrixes due to the solid volume increase of carbonation products upon carbonation. Meanwhile, C-S-H gels surrounding the TiO_2 particles become more porous in hybrid samples due to decalcification, which can alleviate the negative impacts. For samples blended with composite photocatalysts, the alleviation impact is enhanced.
6. The early carbonation of non-fully hydrated cementitious matrixes might hurt the self-cleaning property, and the deterioration is more visible in the OPC-based matrix. Reactive silica can be utilized to promote the instantaneous secondary hydration of CH to C-S-H, then alleviate the deterioration.
7. A mixture recommendation including proper TiO_2 dosage (5 wt%), hybrid binders (cement + reactive silica), and composite photocatalyst (fine reactive silica as the support) is proposed to realize a better resistance to the deterioration of self-cleaning property upon hydration/carbonation.

CRediT authorship contribution statement

Daoru Liu: Methodology, Investigation, Data curation, Formal analysis, Validation, Writing – original draft. **Anna Kaja:** Supervision, Writing – review & editing. **Yuxuan Chen:** Investigation. **H.J.H. Brouwers:** Supervision, Writing – review & editing. **Qingliang Yu:** Conceptualization, Methodology, Funding acquisition, Supervision, Project administration, Writing – review & editing.

Declaration of competing interest

The authors declare that they have no known competing financial interests or personal relationships that could have appeared to influence the work reported in this paper.

Data availability

Data will be made available on request.

Acknowledgments

This research is supported by the National Natural Science Foundation of China (Grant No. 52178246), China Scholarship Council (No. 202006950045) and the Department of the Built Environment at Eindhoven University of Technology. Sincere thanks are given to Weitan Zhuang at Wuhan University (China) for his help with MIP measurements and Dongyu Zhang from the Department of Chemical Engineering and Chemistry at Eindhoven University of Technology.

Appendix A. Supplementary data

Supplementary data to this article can be found online at https://doi.org/10.1016/j.cemconres.2022.107009.

References

[1] M. Bahrar, Z.I. Djamai, M. EL Mankibi, A. Si Larbi, M. Salvia, Numerical and experimental study on the use of microencapsulated phase change materials (PCMs) in textile reinforced concrete panels for energy storage, Sustain. Cities Soc. 41 (2018) 455–468, https://doi.org/10.1016/j.scs.2018.06.014.
[2] S. Cui, C. Ahn, M.C. Wingert, D. Leung, S. Cai, R. Chen, Bio-inspired effective and regenerable building cooling using tough hydrogels, Appl. Energy 168 (2016) 332–339, https://doi.org/10.1016/j.apenergy.2016.01.058.
[3] K. Faraj, M. Khaled, J. Faraj, F. Hachem, C. Castelain, Phase change material thermal energy storage systems for cooling applications in buildings: a review, Renew. Sust. Energ. Rev. 119 (2020), 109579, https://doi.org/10.1016/j.rser.2019.109579.
[4] P. Chindaprasirt, U. Rattanasak, Fabrication of self-cleaning fly ash/polytetrafluoroethylene material for cement mortar spray-coating, J. Clean. Prod. 264 (2020), 121748, https://doi.org/10.1016/j.jclepro.2020.121748.
[5] C.A. Casagrande, W.L. Repette, D. Hotza, Effect of environmental conditions on degradation of NOx gases by photocatalytic nanotitania-based cement mortars after long-term hydration, J. Clean. Prod. 274 (2020), https://doi.org/10.1016/j.jclepro.2020.123067.
[6] K. Ndiaye, S. Ginestet, M. Cyr, Experimental evaluation of two low temperature energy storage prototypes based on innovative cementitious material, Appl. Energy 217 (2018) 47–55, https://doi.org/10.1016/j.apenergy.2018.02.136.

[7] R. Zouzelka, J. Rathousky, Photocatalytic abatement of NOx pollutants in the air using commercial functional coating with porous morphology, Appl. Catal. B Environ. 217 (2017) 466–476, https://doi.org/10.1016/j.apcatb.2017.06.009.

[8] L. Cardellicchio, Self-cleaning and colour-preserving efficiency of photocatalytic concrete: case study of the Jubilee Church in Rome, Build. Res. Inf. 48 (2020) 160–179, https://doi.org/10.1080/09613218.2019.1622405.

[9] J. Chen, C.S. Poon, Photocatalytic cementitious materials: influence of the microstructure of cement paste on photocatalytic pollution degradation, Environ. Sci. Technol. 43 (2009) 8948–8952, https://doi.org/10.1021/es902359s.

[10] P. Munafò, E. Quagliarini, G.B. Goffredo, F. Bondioli, A. Licciulli, Durability of nano-engineered TiO2 self-cleaning treatments on limestone, Constr. Build. Mater. 65 (2014) 218–231, https://doi.org/10.1016/j.conbuildmat.2014.04.112.

[11] A.M. Kaja, H.J.H. Brouwers, Q.L. Yu, NOx degradation by photocatalytic mortars: the underlying role of the CH and C-S-H carbonation, Cem. Concr. Res. 125 (2019), 105805, https://doi.org/10.1016/j.cemconres.2019.105805.

[12] Z. Wang, Q. Yu, F. Gauvin, P. Feng, R. Qianping, H.J.H. Brouwers, Nanodispersed TiO2 hydrosol modified Portland cement paste: the underlying role of hydration on self-cleaning mechanisms, Cem. Concr. Res. 136 (2020), 106156, https://doi.org/10.1016/j.cemconres.2020.106156.

[13] Y. Hendrix, Photocatalytic Abatement of the Nitrogen Oxide Pollution: Synthesis, Application and Long-term Evaluation of Titania-silica Composites, Eindhoven University of Technology, 2020.

[14] C.J. Goodbrake, J.F. Young, R.L. Berger, Reaction of Beta-dicalcium silicate and tricalcium silicate with carbon dioxide and water vapor, J. Am. Ceram. Soc. 62 (1979) 168–171, https://doi.org/10.1111/j.1151-2916.1979.tb19046.x.

[15] D. Wang, J. Chang, Comparison on accelerated carbonation of β-C2S, Ca(OH)2, and C4AF: reaction degree, multi-properties, and products, Constr. Build. Mater. 224 (2019) 336–347, https://doi.org/10.1016/j.conbuildmat.2019.07.056.

[16] Y.X. Chen, Y. Hendrix, K. Schollbach, H.J.H.H. Brouwers, A silica aerogel synthesized from olivine and its application as a photocatalytic support, Constr. Build. Mater. 248 (2020), 118709, https://doi.org/10.1016/j.conbuildmat.2020.118709.

[17] A.A. Essawy, S. Abd, Physico-mechanical properties, potent adsorptive and photocatalytic efficacies of sulfate resisting cement blends containing micro silica and nano-TiO2, Constr. Build. Mater. 52 (2014) 1–8, https://doi.org/10.1016/j.conbuildmat.2013.11.026.

[18] Q.L. Yu, M.M. Ballari, H.J.H. Brouwers, Indoor air purification using heterogeneous photocatalytic oxidation. Part II: kinetic study, Appl. Catal. B Environ. 99 (2010) 58–65, https://doi.org/10.1016/j.apcatb.2010.05.032.

[19] L. Zhang, H.H. Mohamed, R. Dillert, D. Bahnemann, Kinetics and mechanisms of charge transfer processes in photocatalytic systems: a review, J. Photochem. Photobiol. C Photochem. Rev. 13 (2012) 263–276, https://doi.org/10.1016/j.jphotochemrev.2012.07.002.

[20] F. Gauvin, V. Caprai, Q.L. Yu, H.J.H. Brouwers, Effect of the morphology and pore structure of porous building materials on photocatalytic oxidation of air pollutants, Appl. Catal. B Environ. 227 (2018) 123–131, https://doi.org/10.1016/j.apcatb.2018.01.029.

[21] J. Kou, C. Lu, J. Wang, Y. Chen, Z. Xu, R.S. Varma, Selectivity enhancement in heterogeneous photocatalytic transformations, Chem. Rev. 117 (2017) 1445–1514, https://doi.org/10.1021/acs.chemrev.6b00396.

[22] G. Liu, H. Xia, Y. Niu, X. Zhao, G. Zhang, L. Song, H. Chen, Fabrication of self-cleaning photocatalytic durable building coating based on WO3-TNs/PDMS and NO degradation performance, Chem. Eng. J. 409 (2021), 128187, https://doi.org/10.1016/j.cej.2020.128187.

[23] A.V. Zanfir, G. Voicu, A.I. Bădănoiu, D. Gogan, O. Oprea, E. Vasile, Synthesis and characterization of titania-silica fume composites and their influence on the strength of self-cleaning mortar, Compos. Part B Eng. 140 (2018) 157–163, https://doi.org/10.1016/j.compositesb.2017.12.032.

[24] I. Alfieri, A. Lorenzi, L. Ranzenigo, L. Lazzarini, G. Predieri, P.P. Lottici, Synthesis and characterization of photocatalytic hydrophobic hybrid TiO2-SiO2 coatings for building applications, Build. Environ. 111 (2017) 72–79, https://doi.org/10.1016/j.buildenv.2016.10.019.

[25] M. Luna, M.J. Mosquera, H. Vidal, J.M. Gatica, Au-TiO2/SiO2 photocatalysts for building materials: self-cleaning and de-polluting performance, Build. Environ. 164 (2019), https://doi.org/10.1016/j.buildenv.2019.106347.

[26] A. Folli, C. Pade, T.B. Hansen, T. De Marco, D.E. MacPhee, TiO2 photocatalysis in cementitious systems: insights into self-cleaning and depollution chemistry, Cem. Concr. Res. 42 (2012) 539–548, https://doi.org/10.1016/j.cemconres.2011.12.001.

[27] M. Lackhoff, X. Prieto, N. Nestle, F. Dehn, R. Niessner, Photocatalytic activity of semiconductor-modified cement - influence of semiconductor type and cement ageing, Appl. Catal. B Environ. 43 (2003) 205–216, https://doi.org/10.1016/S0926-3373(02)00303-X.

[28] L. Pinho, M.J. Mosquera, Photocatalytic activity of TiO2-SiO2 nanocomposites applied to buildings: influence of particle size and loading, Appl. Catal. B Environ. 134–135 (2013) 205–221, https://doi.org/10.1016/j.apcatb.2013.01.021.

[29] L.D. García, J.M. Pastor, J. Peña, Self cleaning and depolluting glass reinforced concrete panels: fabrication, optimization and durability evaluation, Constr. Build. Mater. 162 (2018) 9–19, https://doi.org/10.1016/j.conbuildmat.2017.11.156.

[30] M. Bellardita, M. Addamo, A. Di Paola, G. Marcì, L. Palmisano, L. Cassar, M. Borsa, Photocatalytic activity of TiO2/SiO2 systems, J. Hazard. Mater. 174 (2010) 707–713, https://doi.org/10.1016/j.jhazmat.2009.09.108.

[31] C. Mendoza, A. Valle, M. Castellote, A. Bahamonde, M. Faraldos, TiO2 and TiO2-SiO2 coated cement: comparison of mechanic and photocatalytic properties, Appl. Catal. B Environ. 178 (2015) 155–164, https://doi.org/10.1016/j.apcatb.2014.09.079.

[32] A. Hakki, L. Yang, F. Wang, D.E. Macphee, The effect of interfacial chemical bonding in TiO2-SiO2 composites on their photocatalytic NOx abatement performance, J. Vis. Exp. 2017 (2017) 1–11, https://doi.org/10.3791/56070.

[33] E. Ghedini, F. Menegazzo, M. Manzoli, A. Di Michele, D. Puglia, M. Signoretto, Multifunctional and environmentally friendly TiO2-SiO2 mesoporous materials for sustainable green buildings, Molecules 24 (2019), https://doi.org/10.3390/molecules24234226.

[34] B. Yu, N. Li, W. He, J. Ji, S. Zhang, H. Chen, Multifunctional solar wall for dehumidification, heating and removal of formaldehyde: part 1. System description, preparation and performance of SiO2/TiO2 adsorbent, Build. Environ. 100 (2016) 203–214, https://doi.org/10.1016/j.buildenv.2016.02.007.

[35] J. Sun, K. Xu, C. Shi, J. Ma, W. Li, X. Shen, Influence of core/shell TiO2@SiO2 nanoparticles on cement hydration, Constr. Build. Mater. 156 (2017) 114–122, https://doi.org/10.1016/j.conbuildmat.2017.08.124.

[36] Y. Sargam, K. Wang, A. Tsyrenova, S. Jiang, F. Liu, Effects of anionic and nonionic surfactants on the dispersion and stability of nanoSiO2 in aqueous and cement pore solutions, Cem. Concr. Res. (2021), 106417, https://doi.org/10.1016/j.cemconres.2021.106417.

[37] X. Ouyang, Y. Guo, X. Qiu, The feasibility of synthetic surfactant as an air entraining agent for the cement matrix, Constr. Build. Mater. 22 (2008) 1774–1779, https://doi.org/10.1016/j.conbuildmat.2007.05.002.

[38] Y. Hendrix, A. Lazaro, Q.L. Yu, H.J.H. Brouwers, Influence of synthesis conditions on the properties of photocatalytic titania-silica composites, J. Photochem. Photobiol. A Chem. 371 (2019) 25–32, https://doi.org/10.1016/j.jphotochem.2018.10.040.

[39] V. Shah, K. Scrivener, B. Bhattacharjee, S. Bishnoi, Changes in microstructure characteristics of cement paste on carbonation, Cem. Concr. Res. 109 (2018) 184–197, https://doi.org/10.1016/j.cemconres.2018.04.016.

[40] H. Taylor, Cement Chemistry, Second Edi, Thomas Telford, London, 1997.

[41] C. Naber, S. Stegmeyer, D. Jansen, F. Goetz-Neunhoeffer, J. Neubauer, The PONKCS method applied for time resolved XRD quantification of supplementary cementitious material reactivity in hydrating mixtures with ordinary Portland cement, Constr. Build. Mater. 214 (2019) 449–457, https://doi.org/10.1016/j.conbuildmat.2019.04.157.

[42] M. Auroy, S. Poyet, P. Le Bescop, J.M. Torrenti, T. Charpentier, M. Moskura, X. Bourbon, Comparison between natural and accelerated carbonation (3% CO2): impact on mineralogy, microstructure, water retention and cracking, Cem. Concr. Res. 109 (2018) 64–80, https://doi.org/10.1016/j.cemconres.2018.04.012.

[43] Y. Sargam, K. Wang, Influence of dispersants and dispersion on properties of nanosilica modified cement-based materials, Cem. Concr. Compos. 118 (2021), 103969, https://doi.org/10.1016/j.cemconcomp.2021.103969.

[44] W.J. Sun, J. Li, G. Mele, Z.Q. Zhang, F.X. Zhang, Enhanced photocatalytic degradation of rhodamine B by surface modification of ZnO with copper (II) porphyrin under both UV-vis and visible light irradiation, J. Mol. Catal. A Chem. 366 (2013) 84–91, https://doi.org/10.1016/j.molcata.2012.09.010.

[45] Y. Zhang, E.K. Stefanakos, D. Yogi Goswami, Effect of photocatalytic surface roughness on reactors effectiveness for indoor air cleaning, Build. Environ. 61 (2013) 188–196, https://doi.org/10.1016/j.buildenv.2012.12.018.

[46] E. Jimenez-Relinque, J.R. Rodriguez-Garcia, A. Castillo, M. Castellote, Characteristics and efficiency of photocatalytic cementitious materials: type of binder, roughness and microstructure, Cem. Concr. Res. 71 (2015) 124–131, https://doi.org/10.1016/j.cemconres.2015.02.003.

[47] T. Watanabe, T. Takizawa, K. Honda, Photocatalysis through excitation of adsorbates. 1. Highly efficient N-deethylation of rhodamine B adsorbed to CdS, J. Phys. Chem. 81 (1977) 1845–1851, https://doi.org/10.1021/j100534a012.

[48] A. Folli, U.H. Jakobsen, G.L. Guerrini, D.E. Macphe, D.E. Macphee, Rhodamine B discolouration on TiO2 in the cement environment : a look at fundamental aspects of the self-cleaning effect in concretes, J. Adv. Oxid. Technol. 12 (2009), https://doi.org/10.1515/jaots-2009-0116, 129-123.

[49] Y. Hendrix, A. Lazaro, Q.L. Yu, H.J.H. Brouwers, Influence of synthesis conditions on the properties of photocatalytic titania-silica composites, J. Photochem. Photobiol. A Chem. 371 (2019) 25–32, https://doi.org/10.1016/j.jphotochem.2018.10.040.

[50] sborschick2012@yandex.ru , Big Chemical Encyclopedia, Chem. Subst. Components, React. Process Des. (n.d.) 614–615. https://chempedia.info/info/ti_o_si_bonding/.

[51] B.Y. Lee, Effect of Titanium Dioxide Nanoparticles on Early Age and Long Term Properties of Cementitious Materials, Georgia Institute of Technology, 2012.

[52] F. Zhou, G. Pan, R. Mi, M. Zhan, Improving the properties of concrete using in situ-grown C-S-H, Constr. Build. Mater. 276 (2021), 122214, https://doi.org/10.1016/j.conbuildmat.2020.122214.

[53] C. Pei, J.H. Zhu, F. Xing, Photocatalytic property of cement mortars coated with graphene/TiO2 nanocomposites synthesized via sol–gel assisted electrospray method, J. Clean. Prod. 279 (2021), 123590, https://doi.org/10.1016/j.jclepro.2020.123590.

[54] M. Pérez-Nicolás, J. Balbuena, M. Cruz-Yusta, L. Sánchez, I. Navarro-Blasco, J. M. Fernández, J.I. Alvarez, Photocatalytic NOx abatement by calcium aluminate cements modified with TiO2: improved NO2 conversion, Cem. Concr. Res. 70 (2015) 67–76, https://doi.org/10.1016/j.cemconres.2015.01.011.

[55] S. Andrade, J. Henrique, P. Cesar, A. Neiry, D.M. Lopes, M. Frías, Investigation of C-S-H in ternary cement pastes containing nanosilica and highly-reactive supplementary cementitious materials (SCMs): microstructure and strength, Constr. Build. Mater. 198 (2019) 445–455, https://doi.org/10.1016/j.conbuildmat.2018.10.235.

[56] U. Sharma, L.P. Singh, B. Zhan, C. Sun, Effect of particle size of nanosilica on microstructure of C-S-H and its impact on mechanical strength, Cem. Concr.

Compos. 97 (2019) 312–321, https://doi.org/10.1016/j.cemconcomp.2019.01.007.
[57] G. Land, D. Stephan, The influence of nano-silica on the hydration of ordinary Portland cement, J. Mater. Sci. 47 (2012) 1011–1017, https://doi.org/10.1007/s10853-011-5881-1.
[60] R. Zhang, X. Cheng, P. Hou, Z. Ye, Influences of nano-TiO2 on the properties of cement-based materials: hydration and drying shrinkage, Constr. Build. Mater. 81 (2015) 35–41, https://doi.org/10.1016/j.conbuildmat.2015.02.003.
[61] S.S. Lucas, V.M. Ferreira, J.L.B. De Aguiar, Incorporation of titanium dioxide nanoparticles in mortars - influence of microstructure in the hardened state properties and photocatalytic activity, Cem. Concr. Res. 43 (2013) 112–120, https://doi.org/10.1016/j.cemconres.2012.09.007.
[62] Z. Shi, B. Lothenbach, M.R. Geiker, J. Kaufmann, A. Leemann, S. Ferreiro, J. Skibsted, Experimental studies and thermodynamic modeling of the carbonation of Portland cement, metakaolin and limestone mortars, Cem. Concr. Res. 88 (2016) 60–72, https://doi.org/10.1016/j.cemconres.2016.06.006.
[63] M. Arandigoyen, B. Bicer-Simsir, J.I. Alvarez, D.A. Lange, Variation of microstructure with carbonation in lime and blended pastes, Appl. Surf. Sci. 252 (2006) 7562–7571, https://doi.org/10.1016/j.apsusc.2005.09.007.
[64] T. Chen, X. Gao, L. Qin, Mathematical modeling of accelerated carbonation curing of Portland cement paste at early age, Cem. Concr. Res. 120 (2019) 187–197, https://doi.org/10.1016/j.cemconres.2019.03.025.
[65] B.Z. Dilnesa, Application of thermogravimetric method in cement science. https://www.empa.ch/documents/55996/231904/Poster-Application+of+thermogravimetric.pdf/cd759220-84e7-48e1-910e-c131280be061, 2020.
[66] P.H.R. Borges, J.O. Costa, N.B. Milestone, C.J. Lynsdale, R.E. Streatfield, Carbonation of CH and C-S-H in composite cement pastes containing high amounts of BFS, Cem. Concr. Res. 40 (2010) 284–292, https://doi.org/10.1016/j.cemconres.2009.10.020.
[67] T. Kim, J. Olek, Effects of sample preparation and interpretation of thermogravimetric curves on calcium hydroxide in hydrated pastes and mortars, Transp. Res. Rec. (2012) 10–18, https://doi.org/10.3141/2290-02.
[68] A. Cuesta, I. Santacruz, A.G. De la Torre, M. Dapiaggi, J.D. Zea-Garcia, M.A. G. Aranda, Local structure and Ca/Si ratio in C-S-H gels from hydration of blends of tricalcium silicate and silica fume, Cem. Concr. Res. 143 (2021), 106405, https://doi.org/10.1016/j.cemconres.2021.106405.
[69] P.R. Jubu, F.K. Yam, V.M. Igba, K.P. Beh, Tauc-plot scale and extrapolation effect on bandgap estimation from UV–vis–NIR data – a case study of β-Ga2O3, J. Solid State Chem. 290 (2020), 121576, https://doi.org/10.1016/j.jssc.2020.121576.
[70] M. Kang, S.W. Kim, H.Y. Park, Optical properties of TiO2 thin films with crystal structure, J. Phys. Chem. Solids 123 (2018) 266–270, https://doi.org/10.1016/j.jpcs.2018.08.009.
[71] V. Nadtochenko, N. Denisov, A. Gorenberg, Y. Kozlov, P. Chubukov, J.A. Rengifo, C. Pulgarin, J. Kiwi, Correlations for photocatalytic activity and spectral features of the absorption band edge of TiO2 modified by thiourea, Appl. Catal. B Environ. 91 (2009) 460–469, https://doi.org/10.1016/j.apcatb.2009.06.015.
[72] R. López, R. Gómez, Band-gap energy estimation from diffuse reflectance measurements on sol-gel and commercial TiO 2: a comparative study, J. Sol-Gel Sci. Technol. 61 (2012) 1–7, https://doi.org/10.1007/s10971-011-2582-9.
[73] F. Sieland, N.A.T. Duong, J. Schneider, D.W. Bahnemann, Influence of inorganic additives on the photocatalytic removal of nitric oxide and on the charge carrier dynamics of TiO2 powders, J. Photochem. Photobiol. A Chem. 366 (2018) 142–151, https://doi.org/10.1016/j.jphotochem.2018.01.036.
[74] J.M. Marr, F.P. Wilkin, A better presentation of Planck's radiation law, Am. J. Phys. 80 (2012) 399–405, https://doi.org/10.1119/1.3696974.
[75] S. Karapati, T. Giannakopoulou, N. Todorova, N. Boukos, S. Antiohos, D. Papageorgiou, E. Chaniotakis, D. Dimotikali, C. Trapalis, TiO 2 functionalization for efficient NOxremoval in photoactive cement, Appl. Surf. Sci. 319 (2014) 29–36, https://doi.org/10.1016/j.apsusc.2014.07.162.
[76] E. Jimenez-Relinque, I. Llorente, M. Castellote, TiO2 cement-based materials: understanding optical properties and electronic band structure of complex matrices, Catal. Today 287 (2017) 203–209, https://doi.org/10.1016/j.cattod.2016.11.015.
[77] M. Nolan, Surface modification of TiO2 with metal oxide nanoclusters: a route to composite photocatalytic materials, Chem. Commun. 47 (2011) 8617–8619, https://doi.org/10.1039/c1cc13243a.
[78] N. Guijarro, M.S. Prévot, K. Sivula, Surface modification of semiconductor photoelectrodes, Phys. Chem. Chem. Phys. 17 (2015) 15655–15674, https://doi.org/10.1039/c5cp01992c.
[79] S. Adachi, Optical Properties of Crystalline and Amorphous Semiconductors: Materials and Fundamental Principles, Springer Science+Business Media, LLC, Gunma Prefecture, Japan, 1999, https://doi.org/10.1007/978-1-4615-5241-3.
[80] J.A. Larbi, J.M.J.M. Bijen, Interaction of polymers with Portland cement during hydration. A study, Cem. Concr. Res. 20 (1990) 139–147.
[81] H.J.H. Brouwers, R.J. VanEijk, Alkali concentrations of pore solution in hydrating OPC, Cem. Concr. Res. 33 (2003) 191–196, https://doi.org/10.1016/S0008-8846(02)01022-0.
[82] V.K. Ortolan, M. Mancio, B.F. Tutikian, Evaluation of the influence of the pH of concrete pore solution on the corrosion resistance of steel reinforcement, J. Build. Pathol. Rehabil. 1 (2016) 1–7, https://doi.org/10.1007/s41024-016-0011-8.
[83] Byfors Kajsa, Influence of silica fume and flyash on chloride diffusion, Cem. Concr. Res. 17 (1987) 115–130.
[84] L. J.A, The chemistry of the pore fluid of silica fume-blended cement systems, Cem. Concr. Res. 20 (1990) 506–516, https://doi.org/10.1016/0008-8846(90)90095-F.
[85] R. Qian, Y. Zhang, C. Liu, Z. Liu, Y. Zhang, G. Liu, Effects of supplementary cementitious materials on pore-solution chemistry of blended cements, J. Sustain. Cem. Mater. (2021) 1–27, https://doi.org/10.1080/21650373.2021.1988754.
[86] E. Bernard, Y. Yan, B. Lothenbach, Effective cation exchange capacity of calcium silicate hydrates (C-S-H), Cem. Concr. Res. 143 (2021), 106393, https://doi.org/10.1016/j.cemconres.2021.106393.
[87] X. Zhu, S.R. Castleberry, M.A. Nanny, E.C. Butler, Effects of pH and catalyst concentration on photocatalytic oxidation of aqueous ammonia and nitrite in titanium dioxide suspensions, Environ. Sci. Technol. 39 (2005) 3784–3791, https://doi.org/10.1021/es0485715.
[88] L. Zhong, F. Haghighat, Photocatalytic air cleaners and materials technologies - abilities and limitations, Build. Environ. 91 (2015) 191–203, https://doi.org/10.1016/j.buildenv.2015.01.033.
[89] L. Black, K. Garbev, I. Gee, Surface carbonation of synthetic C-S-H samples: a comparison between fresh and aged C-S-H using X-ray photoelectron spectroscopy, Cem. Concr. Res. 38 (2008) 745–750, https://doi.org/10.1016/j.cemconres.2008.02.003.
[90] W. Kurdowski, The protective layer and decalcification of C-S-H in the mechanism of chloride corrosion of cement paste, Cem. Concr. Res. 34 (2004) 1555–1559, https://doi.org/10.1016/j.cemconres.2004.03.023.
[91] A. Morandeau, M. Thiéry, P. Dangla, Investigation of the carbonation mechanism of CH and C-S-H in terms of kinetics, microstructure changes and moisture properties, Cem. Concr. Res. 56 (2014) 153–170, https://doi.org/10.1016/j.cemconres.2013.11.015.
[92] Z. Liu, W. Meng, Fundamental understanding of carbonation curing and durability of carbonation-cured cement-based composites: a review, J. CO2 Util. 44 (2021), 101428, https://doi.org/10.1016/j.jcou.2020.101428.
[93] R.D. Moser, C.A. Weiss, Applied Mineralogy of Cement & Concrete, 2014, https://doi.org/10.2138/am.2014.622.
[94] Y. Li, W. Liu, F. Xing, S. Wang, L. Tang, S. Lin, Z. Dong, Carbonation of the synthetic calcium silicate hydrate (C-S-H) under different concentrations of CO2: chemical phases analysis and kinetics, J. CO2 Util. 35 (2020) 303–313, https://doi.org/10.1016/j.jcou.2019.10.001.